2. Theoretical Concepts of Lasers

2.1. Basics of Laser Modelling

Lasers are light sources with very narrow bandwidths, high output power and long coherence lengths [HAK86]. They are, in some regards, completely different from other light sources, that surround us every day. As opposed to the thermal radiation of light bulbs, stars and the sun, or the fluorescence used in neon tubes, the photons of a laser are mainly emitted through *stimulated emission*.

This section will explain the basic concepts of a laser and present a simple numerical model to show some general laser dynamics.

2.1.1. Basic Concepts

When in the early 20th century the particle-like nature of light was discovered and Niels Bohr formulated the famous Bohr model of the atom, two types of light-matter interactions were soon understood. Firstly, spontaneous emission is the stochastic decay of an excited electron, where a photon is emitted during the electrons transition from an upper state with energy E_2 to a lower energetic state of energy E_1. Secondly, an incoming photon of matching energy $\hbar\omega = E_2 - E_1$ can be absorbed while lifting the electron from the lower to the higher state.

However, Albert Einstein proposed the existence of an additional interaction, namely *stimulated emission*, in 1917 [EIN17]. There, an incoming photon of matching energy $\hbar\omega = E_2 - E_1$ is not absorbed, but encounters the electron in the upper state and stimulates the decay into the lower state. Hence, a second photon is emitted, which is identical in phase and direction to the first one. On a macroscopic scale the light intensity is coherently amplified by this process. Figure 2.1 shows a sketch of the three single-photon processes described above.

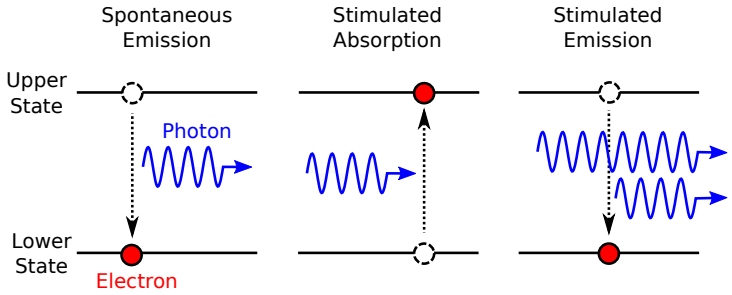

Figure 2.1: Sketch of the three fundamental single-photon interactions of a two-level system. For spontaneous emission (a), an electron (red) decays from the upper energetic state to the lower energetic state, while emitting a photon (blue). Conversely, through stimulated absorption (b) an electron is lifted into the upper state, while a photon is simultaneously consumed. Lastly, stimulated emission (c) is the coherent emission of a second photon, by an incoming photon that finds the electron in the upper state.

A. Röhm, *Dynamic Scenarios in Two-State Quantum Dot Lasers,* BestMasters,
DOI 10.1007/978-3-658-09402-7_2, © Springer Fachmedien Wiesbaden 2015

Through simple calculus [HAK86] Einstein could also show that the light-matter interaction coefficients, nowadays called in his honour Einstein-coefficients, had to be identical for stimulated emission and absorption. Stimulated emission is therefore often seen as the reverse process of (stimulated) absorption. Followingly, a net amplification of incoming light can only be achieved by stimulated emission, if more electrons are available for stimulated emission than for absorption, ergo if the population N of the upper state is higher than of the lower state, $N_2 > N_1$.

Yet, this state of 'population inversion' is never reached in thermal equilibrium. Mathematically, the Maxwell-Boltzmann-distribution only allows states with higher energies to be filled more, if the temperature is set to a negative value [HAK86]. Population inversion is therefore sometimes also referred to as 'negative temperature', albeit macroscopic systems never reach negative temperatures as a stable equilibrium state.

Hence, the system must be constantly driven out of thermal equilibrium to achieve 'population inversion'. This process called 'pumping' can be achieved through various ways and depends on the system being used. It can be optically, electrically or even chemically driven [HAK86]. Some pumping mechanisms will only provide sufficient inversion for a very short time leading to pulsed lasers, while others allow the emission of a continuous wave. Furthermore, even though only two energetic levels are participating in the optical transition, all real-world lasers do incorporate at least three different energy levels, often even four, and are congruently referred to as three-level lasers and four-level lasers [ERN10b]. A sketch of the pumping and lasing transitions of these systems is shown in Fig. 2.2.

The advantage of involving additional states for the electrons are easy to understand: While an optically driven two-level system can never reach population inversion through optical pumping, as the absorption and stimulated emission balance each other out, the three-level system avoids this by indirect excitation. The electrons are lifted from the lowest level of energy E_1 to a level above the upper level involved in the transition. In a suitable material, the electrons in this state of energy $E_3 > E_2$ then quickly decay into the upper state of energy E_2 of the lasing transition. An effective pumping without disturbing level 2 is therefore possible. Yet, to reach population inversion at least half of the population of level 1 would still have to be excited. This strict requirement is lifted for the four-level laser.

In the four-level system of energies $E_1 < E_2 < E_3 < E_4$, the electrons are lifted from the level 1 in to the level 4 through pumping, quickly decay into the metastable level 3, where they are used for stimulated emission, similar to the three-level system. However, in the optimal case the transition from energy level 2 to 1 is extremely fast, leaving the level 2 constantly almost empty and followingly keeping a population inversion between levels 2 and 3. Overall, the pumping requirements for lasing operations are greatly reduced and hence four-level systems are common [ERN10b, HAK85]. Figure 2.2 shows pumping and transition schemes for the three-level and four-level system.

Quantum dot lasers can be seen as a four-level system, with the conduction band and valence band acting as the highest and lowest level, while the quantum dot levels encompass the optically active lasing transition. However, the complex scattering

dynamics involved lead to a variety of additional effects, e.g. two-state lasing or ground state quenching.

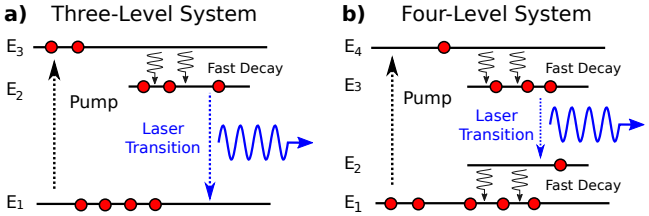

Figure 2.2: Sketch of the pumping and energy level scheme for the three-level laser (a) and four-level laser (b). Electrons (red) are raised by the pump to the highest energetic level, from which they quickly decay into the upper state of the lasing transition. This state is ideally metastable, so that electrons can accumulate there. For the three-level system (a), the lasing transition then links this metastable state E_2 to the ground level E_1. The four-level laser (b) possesses an additional level E_2, that acts as the lower state for the lasing transition. Because this level E_2 is short lived, it is almost always empty, leaving the E_3-E_2 transition easily inverted.

From an engineering perspective, the laser converts the energy injected into the system via pumping, e.g. the injection current in a semiconductor laser, into coherent light. One can therefore easily formulate conversion efficiencies by measuring the output versus input power. Electrically driven semiconductor lasers are among the most efficient lasing systems [CHO99].

Mathematically, the amplification of an incoming electro-magnetic wave is often measured as *gain* g. In a simple model the electric field amplitude E will increase exponentially over time with gain g:

$$\frac{d}{dt}E = gE. \tag{2.1}$$

Gain is therefore quantified in units of [1/s]. Microscopically, the gain of a medium is related to its population inversion:

$$g \sim N_2 - N_1, \tag{2.2}$$

where N_2 and N_1 are the populations of the upper and lower electronic level. When the lower level is more populated, the gain g becomes negative and instead of amplifying the incoming wave, the medium becomes absorbing. Gain g can therefore also be seen as an inverse absorption coefficient. The interplay of gain and light will be discussed in more detail in the following section.

2.1.2. Cavity and Active Medium

The two principal components of every laser are the *optical cavity* and the optically active *gain medium* [HAK85] contained inside. The cavity is a confined space in

which certain standing electromagnetic waves can exist. These 'cavity modes' have a discrete set of eigenfrequencies and can be excited via injection of photons. Typically the edge of the cavity will be a mirror or another reflecting surface, so that photons of the cavity modes are reflected. The light then passes through the gain medium multiple times before being absorbed or escaping the cavity. The gain medium is a material, which amplifies light through the process of stimulated emission in the manner described in the previous section. When placed in a cavity, it will be exposed to its own amplified emission and create a coherent, intensity amplified standing wave. This is the origin of the name laser, an acronym for 'Light Amplification by Stimulated Emission of Radiation'.

However, the gain medium does not enhance all optical frequency equally, but possesses a gain profile. This gain profile usually corresponds to the spontaneous emission spectrum of the optical transition that is used for amplification, e.g. a Gaussian shape with its natural line width. For lasers there are usually many cavity modes lying within the peak of the gain spectrum, so that the laser, in principle, could operate on many different modes. Hence, further mode selections becomes necessary.

One easy way of mode selection is to use a Fabry-Perot resonator, as proposed by Schawlow and Townes [SCH58] in 1958. There, only modes along the principal axis of the resonator are enhanced. It consists of two parallel mirrors and significantly reduces the number of modes remaining inside the gain spectrum for optical amplification. A sketch of a Fabry-Perot type laser with all integral components can be seen in Fig. 2.3. Additionally, the coherent light has to be coupled out of the cavity for further use. This is achieved by using a high-reflectivity mirror on one side, and a low reflectivity mirror on the other. Light will then be mainly exiting through the low reflective end of the cavity.

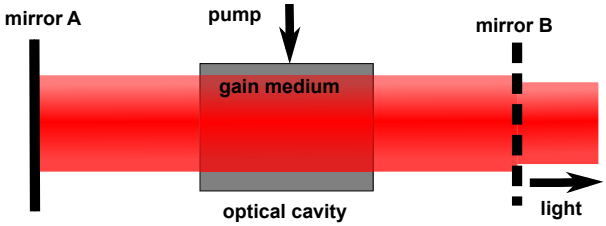

Figure 2.3: Sketch of a Fabry-Perot type laser. The cavity, also called optical resonator, consists of two planar parallel mirrors. The reflectivity of mirror B is lower than of mirror A, so that light mainly leaves the cavity on this side. Inside is the gain medium, which is kept in a state of inversion via pumping. Stimulated emission leads to the appearance of one stable coherent standing wave mode inside the resonator.

In this work the focus lies on the Fabry-Perot type of devices, and it will be assumed that only one lasing mode exists, corresponding to the mode with the highest optical amplification. Excluding the multi-mode dynamics not only decreases computational costs and complexity, but is also consistent with most fabricated QD laser structures, e.g. those with distributed Bragg-reflectors (DBRs). Usually, the end

of the semiconductor sample is simply cleaved and the resulting air-bulk material interface is used as a mirror, resulting in a Farby-Perot type cavity. The alignment is automatically generated by splitting both ends among the same crystallographic plane.

2.1.3. Laser Rate Equations

There are many ways of mathematically describing a laser, suited for different material systems, time scales and types of lasers. However, some laser properties are universal and can hence be understood with even the simplest model approach.

Before the semiclassical laser-equations will be derived in the next section, a simple two-variable rate-equation model shall be heuristically motivated and studied here. The specific set of differential equations are taken from T. Erneux and P. Glorieux [ERN10b] and represent such a minimal laser model. They are given by:

$$\begin{aligned} \frac{d}{dt}I &= ID - I \\ \frac{1}{\gamma}\frac{d}{dt}D &= (A - D) - DI, \end{aligned} \tag{2.3}$$

where I is the light intensity and D is the inversion of the gain medium. Both dynamic variables are normalised, to have as few parameters remaining as possible. As can be seen, the time evolution of the light intensity $\frac{d}{dt}I$ contains a normalised decay term $-I$, which models the loss of light due to absorption and transmission at the mirrors. Furthermore, the product term ID simulates the stimulated emission, which is stronger for more light and higher population inversion and hence linear in both I and D.

This increase in light intensity translates into a loss of inversion D, as stimulated emission uses up excited carriers. Therefore, $-ID$ enters the time evolution of D as a loss term. Additionally, the inversion is being externally driven towards a static value, prescribed by the pump parameter A. The specific nature of the pump is not further specified - it is simply assumed that through some mechanism the inversion of the gain medium can be excited. Lastly, γ is a parameter describing the time scale separation between carrier and light dynamics, usually in the range of 10^{-2} to 10^{-6} [ERN10b].

Now, it is easy to find the steady states of this simplified system by solving the equations:

$$\begin{aligned} ID - I &= 0 \\ (A - D) - DI &= 0. \end{aligned} \tag{2.4}$$

There are two sets of steady states fulfilling these conditions. The first is given by:

$$\begin{aligned} I^{off} &= 0 \\ D^{off} &= A. \end{aligned} \tag{2.5}$$

With the light intensity I at zero and the inversion D at pump level, this represents an 'off'-state. No intensity is produced and carriers are dominated by the external pumping A. Conversely, the second steady state solution of Eq. (2.4) yields the 'on'-state:

$$\begin{aligned} I^{on} &= A - 1 \\ D^{on} &= 1. \end{aligned} \tag{2.6}$$

Here, the light intensity I is proportional to the pump parameter A, caused by the conversion of injected energy into lasing light. Simultaneously the inversion is constant with $D^{on} = 1$. This effect is called *gain clamping* and is a result of the stimulated emission dominating the system. As can be seen from the differential equation for I, $D = 1$ is the transparent state of the system, where the stimulated emission and optical losses cancel each other out.

Now, a linear stability analysis of the system can be calculated. The Jacobian $\underline{\underline{J}}$ of Eq. (2.3) is given by:

$$\underline{\underline{J}} = \begin{bmatrix} D - 1 & I \\ \gamma D & \gamma(-1 - I). \end{bmatrix} \tag{2.7}$$

With this Jacobian, the time evolution of small perturbations δI and δD around the steady states can be described:

$$\begin{aligned} \delta I &= I - I^{on,off} \\ \delta D &= D - D^{on,off} \\ \frac{d}{dt}\begin{pmatrix} \delta I \\ \delta D \end{pmatrix} &= \underline{\underline{J}}\begin{pmatrix} \delta I \\ \delta D \end{pmatrix} + \mathcal{O}\left(\delta I^2, \delta D^2\right), \end{aligned} \tag{2.8}$$

where a vector notation was used for δD and δI. The linear differential Eq. (2.8) can be solved with a two-exponential ansatz:

$$\begin{pmatrix} \delta I \\ \delta D \end{pmatrix} = \begin{pmatrix} a_1 \\ a_2 \end{pmatrix} e^{\lambda_1 t} + \begin{pmatrix} b_1 \\ b_2 \end{pmatrix} e^{\lambda_2 t}, \tag{2.9}$$

where a and b are coefficients for the initial value, and $\lambda_{1,2}$ are the eigenvalues of the Jacobian $\underline{\underline{J}}$. Now, when the steady state variables $I^{on,off}$ and $D^{on,off}$ are inserted, the eigenvalues of the resulting matrix can be easily calculated. For the off-state they are:

$$\lambda_1^{off} = A - 1$$
$$\lambda_2^{off} = -\gamma. \tag{2.10}$$

For values of $A < 1$, both eigenvalues are negative. Following Eq. (2.9) this means that all small perturbations δI and δD decay exponentially, so that the steady state is stable. Conversely, for values of $A > 1$, hence for stronger pumping, the *off*-state becomes unstable. The eigenvalues for the *on*-state are given by:

$$\lambda_{1,2}^{on} = -\gamma\frac{A}{2} \pm \sqrt{\gamma^2 A^2/4 - \gamma(A-1)}, \tag{2.11}$$

for which the plus-combination changes sign. For $A < 1$ the *on*-state is unstable, while for $A > 1$ it is stable. Figure 2.4 shows the steady state solutions of Eq. (2.5) and Eq. (2.6). The *off*-state and *on*-state exchange stability in a transcritical bifurcation at $A = 1$.

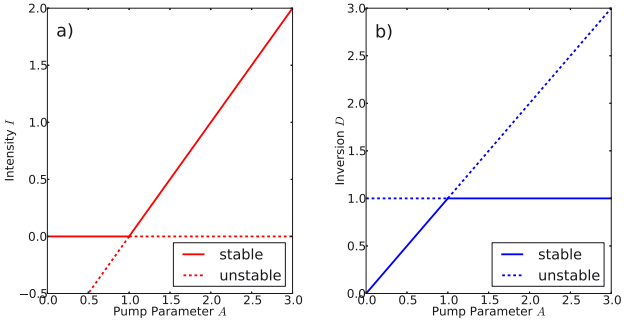

Figure 2.4: Steady states of the rate equation model, (a) intensity I and (b) inversion D against pump parameter A. The stable solutions (solid lines) switch in a transcritical bifurcation at $A = 1$. For $A < 1$ the laser is turned off ($I = 0$) and inversion increases linear with the pump A. The *on*-state is stable for $A = 1$, and $D = 1$ is *gain-clamped*.

As the lasing intensity (a) is zero before, and increases linearly afterwards, $A = 1$ is called the *lasing threshold* and is a typical feature of laser dynamics. On the lasing threshold the system undergoes a change of stability and the state of the system is qualitatively different afterwards. For this simple two-variable rate equation approach here the intensity is zero below threshold and this drastic transition is followingly quite obvious, but even in more complex systems with spontaneous emission included, a pump current corresponding to the lasing threshold can be identified [ERN10b]. It marks the transition towards stimulated emission and the onset of coherent light emission.

Figure 2.4 (b) also shows the *gain clamping* of the inversion and visualises the lasing threshold in terms of carrier dynamics. So while for $A < 1$ the inversion increases

linearly with pump A, which is the result of more electrons getting excited through the pumping mechanism, this rise is suddenly stopped at the lasing threshold $A = 1$. As mentioned, for $D = 1$ the stimulated emission cancels out the decay of intensity I, so that the lasing intensity is stable. If the system were to reach a state of $D > 1$, this would result in an amplification of I through stimulated emission. However, an increased lasing intensity I also increases the losses that the stimulated emission term $-DI$ represents for the time evolution of D in Eq. (2.3). So while the lasing intensity goes up, inversion is consumed simultaneously. Followingly, there are no steady states with $D > 1$, as any excess inversion is always converted into increased light intensity.

Gain clamping above the lasing threshold is a key feature of all lasing systems. If enough carriers get excited, the stimulated emission will start to dominate the system. This always suppresses the participating inversion to a state of transparency, where stimulated emission and optical losses cancel each other out.

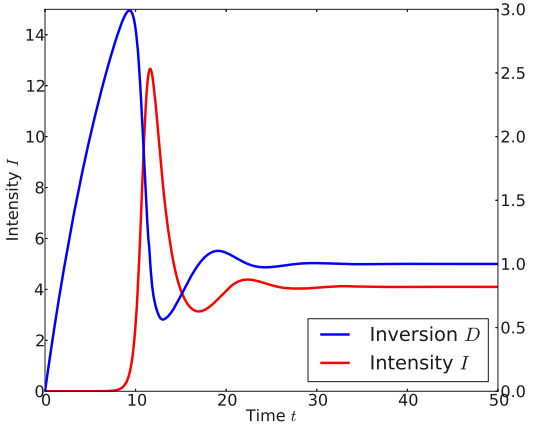

Figure 2.5: Turn-on time series for the set of rate equations obtained by numerical integration. For pump parameter $A = 5.1$ and $\gamma = 10^{-1}$ relaxation oscillations are clearly visible, caused by the periodic interaction of intensity I (red) and inversion D (blue).

Lastly, for $\gamma < 1$ the eigenvalues of Eq. (2.11) turn into a pair of complex conjugated eigenvalues. So the *on*-state is actually a stable focus. This gives rise to *relaxation oscillations*, which is the periodic exchange of energy between gain medium and light field during turn-on. Figure 2.5 plots the turn-on for the rate equation model above threshold ($A = 5.1$) for $\gamma = 10^{-1}$. Both the inversion D and intensity I clearly overshoot and then exhibit damped oscillations before converging towards their steady state values.

The frequency ω_{osc} and damping Γ of the relaxation oscillations is given by the real and imaginary part of the eigenvalue of Eq. (2.11):

$$\Gamma = \gamma \frac{A}{2}. \tag{2.12}$$

The damping increases linearly with pump A, while the frequency can be expanded for small γ to [ERN10b, OTT14]:

$$\begin{aligned}\omega_{osc} =& \sqrt{-\gamma^2 A^2/4 + \gamma(A-1)},\\ \simeq& \sqrt{\gamma(A-1)} + \mathcal{O}(\gamma^{3/2}).\end{aligned} \tag{2.13}$$

Hence, relaxation oscillations are slowest at the threshold $A = 1$, but also least damped. This result once again is also true for more complex laser systems[LUE11]. Semiconductor lasers also exhibit relaxation oscillations, which can be used for the generation of short pulses by gain-switching[SCH88j]. However, the relaxation oscillations of QD semiconductor lasers as studied in this work are often so strongly damped [ERN10b], that they are not even visible. This is important for a range of properties, e.g. their stability against perturbations and modulation dynamics.

Overall, such a simple rate-equation model is useful for outlining and visualising a variety of general laser properties. However, two-state lasing quantum dots are not reproducible, as one needs to include more carrier reservoirs and lasing fields. Furthermore, a theoretical description should be derived from first principles, to ensure that all important aspects are taken into account and experiments can be accurately modelled. Therefore, the next section will cover the semiclassical laser-equations.

2.2. Semiclassical Laser Theory

2.2.1. Field Equations

To accurately model a semiconductor laser, equations of motions for the electric field and the internal states of the gain medium must be derived from first principles. Because the number of photons is very large, it is sufficient [LIN11b, MEY91] to treat the field equations classically for most applications, while the gain medium is treated in the framework of quantum mechanics. This leads to the Maxwell-Bloch equations of semiclassical laser theory.

First, the field dynamics shall be derived. As a starting point, Maxwell's equation in matter are given by [HAK86]:

$$\mathrm{div}\boldsymbol{D} = \rho, \tag{2.14}$$

$$\mathrm{div}\boldsymbol{B} = 0, \tag{2.15}$$

$$\mathrm{rot}\boldsymbol{E} = -\dot{\boldsymbol{B}}, \tag{2.16}$$

$$\mathrm{rot}\boldsymbol{H} = \boldsymbol{j} + \dot{\boldsymbol{D}}. \tag{2.17}$$

Here $\boldsymbol{B}$ and $\boldsymbol{E}$ are the magnetic induction and electric field strength. ρ is the density of free electric charge carriers, $\boldsymbol{j}$ the corresponding current density. The dielectric displacement $\boldsymbol{D}$ is connected to $\boldsymbol{E}$ via

$$\boldsymbol{D} = \epsilon_0 \boldsymbol{E} + \boldsymbol{P_{all}}, \tag{2.18}$$

where ϵ_0 is the vacuum permittivity and $\boldsymbol{P_{all}}$ the polarization of the medium. The polarization will now be split into a resonant part $\boldsymbol{P_r}$ and an off-resonant background polarization $\boldsymbol{P_{bg}}$:

$$\boldsymbol{P_{all}} = \boldsymbol{P_r} + \boldsymbol{P_{bg}}. \tag{2.19}$$

While the resonant polarization $\boldsymbol{P_r}$ will need to be modelled microscopically, the off-resonant polarization $\boldsymbol{P_{bg}}$ is assumed to act linearly during laser operation:

$$\boldsymbol{P_{bg}} = \epsilon_0 \chi_{bg} \boldsymbol{E}, \tag{2.20}$$

and will be absorbed into $\epsilon_{bg} = 1 + \chi_{bg}$. For non-magnetic materials, the magnetizing field $\boldsymbol{H}$ is given by

$$\boldsymbol{B} = \mu_0 \boldsymbol{H}. \tag{2.21}$$

With no free charge carriers $\rho = 0$ and no free current $\boldsymbol{j} = 0$ the Equation for the electric field can be derived as:

$$\Delta \boldsymbol{E} - \frac{n^2}{c^2} \ddot{\boldsymbol{E}} = \mu_0 \ddot{\boldsymbol{P}}, \tag{2.22}$$

where the subscript of $\boldsymbol{P_r}$ has been suppressed and the relation $n^2 c^{-2} = (\epsilon_0 \epsilon_{bg} \mu_0)^{1/2}$ was used. Here, c denotes the vacuum speed of light, while $n = \sqrt{\epsilon_{bg}}$ is the refractive index of the medium and $\Delta = \partial_x^2 + \partial_y^2 + \partial_z^2$ denotes the Laplace-operator.

To further simplify, it will now be assumed that the electric field $\boldsymbol{E}$ can be approximated as a plane wave in z-direction with frequency ω, wave number k and envelope amplitude function $E(t)$. This is justified, as the laser possesses a dominant direction and inside the resonator standing waves are formed. A corresponding approach is taken for the polarization $\boldsymbol{P}$:

$$\boldsymbol{E}(z,t) = \hat{\boldsymbol{e}}_{\boldsymbol{x}} E(t) \exp\left[i\left(kz - \omega t\right)\right] \tag{2.23}$$

$$\boldsymbol{P}(z,t) = \hat{\boldsymbol{e}}_{\boldsymbol{x}} P(t) \exp\left[i\left(kz - \omega t\right)\right] \tag{2.24}$$

Here, $\hat{e}_x$ denotes a constant unit vector in the direction of polarization and $E(t)$ is the time-dependent electric field amplitude. After inserting Eq. (2.23) and Eq. (2.24) into Eq. (2.22) the following equation for E and P is obtained:

$$k^2 E - \frac{n^2}{c^2}(\ddot{E} - 2i\omega\dot{E} - \omega^2 E) = -\mu_0 \left(\ddot{P} - 2i\omega\dot{P} - \omega^2 P\right). \tag{2.25}$$

Now the dispersion relation in matter is used:

$$k^2 = \frac{\omega^2 n^2}{c^2}, \tag{2.26}$$

which leads to the following equation of motion for the envelope function of polarization P and electric field E:

$$\ddot{E}(t) - 2i\omega\dot{E} = -\frac{1}{\epsilon_0\epsilon_{bg}}\left(\ddot{P}(t) - 2\omega\dot{P} - \omega^2 P(t)\right) \tag{2.27}$$

Now, the slowly varying envelope approximation (SVEA) will be applied [HAK85], which uses the fact that the envelope function does not change significantly during one period T_{opt} of the fast optical oscillation,

$$|\dot{E}| \ll \omega|E| = \frac{2\pi}{T_{opt}}|E|, \tag{2.28}$$

so that only the terms of lowest order dominate Eq. (2.27) and the other can be neglected. The equation for the electric field amplitude E then is:

$$\frac{\mathrm{d}E}{\mathrm{d}t} = \frac{i\omega\Gamma}{2\epsilon_0\epsilon_{bg}}P, \tag{2.29}$$

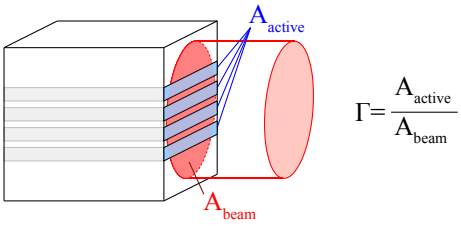

Figure 2.6: Sketch of the confinement factor used in calculating the mode volume in a semiconductor laser. The confinement factor quantifies the overlap between electric field (red area) and active medium (blue layers).

where the confinement factor Γ was include. The confinement factor is a phenomenological addition and quantifies the fraction of the electric field overlapping with the gain medium in the laser (see Fig. 2.6), because in a semiconductor laser the extent of the standing electric field is usually bigger than the active region, i.e. the QD layer. Higher confinement leads to a more concentrated electric field profile and can be achieved by wave guiding. This results in a stronger interaction between the QDs and the light, but can also damage the semiconductor material, if intensities surpass the damage threshold of the material.

2.2.2. Matter Equations

After the field equations could be derived, the light-matter interaction and internal dynamics of the gain medium need to be described. To do so, it is necessary to derive the macroscopic polarization $\boldsymbol{P}$ as a function of the internal state of the gain medium [HAK85, CHO99]. On a fundamental level, the electric field is interacting with an optical transition, which needs to be inverted to facilitate lasing. This optical transition is in the most basic form a two-level system of electronic states, between which a transition is possible.

This can be described in the framework of quantum mechanics, of which the representation in second quantization will be used here. Furthermore, the electric field $\boldsymbol{E}$ is still described classically and not in the form of quantum electrodynamics. Without derivation, the Hamiltonian $\hat{H}$ for such a system is given by [CHO99]:

$$\begin{aligned}\hat{H} = H_0 + H_s = &\sum_{\alpha_j} \epsilon_{\alpha_j} a^\dagger_{\alpha_j} a_{\alpha_j} + \sum_{\beta_j} \epsilon_{\beta_j} b^\dagger_{\beta_j} b_{\beta_j} \\ &- \sum_{\alpha_j,\beta_j} (\mu_{\alpha_j\beta_j} a^\dagger_{\alpha_j} b^\dagger_{\beta_j} + \mu^*_{\alpha_j\beta_j} a_{\alpha_j} b_{\beta_j}) \mathrm{Re}(E(t) e^{-i\omega t}). \end{aligned} \tag{2.30}$$

It consists of two parts, the single-state energies H_0 and the interaction H_s. α_j and β_j are sets of suitable quantum numbers for the upper and lower electronic levels, e.g. spin or wave number k. Then, a_{α_j} is the creation operator for an electron in the upper state and the hermitian conjugate $a^\dagger_{\alpha_j}$ the corresponding annihilation operator. Conversely, b_{β_j} and $b^\dagger_{\beta_j}$ are the creation and annihilation operator for holes in the lower state.

The number operators $a^\dagger_{\alpha_j} a_{\alpha_j}$ and $b^\dagger_{\beta_j} b_{\beta_j}$ count the number of electrons and holes, respectively. Together with the single particle state energies ϵ_{α_j} and ϵ_{β_j} the first two terms of Eq. (2.30) account for the energy of all occupied states. The last term describes the interaction with the electric field of amplitude E and frequency ω. Here, $\mu_{\alpha_j\beta_j}$ denotes the transition matrix element between state α_j and β_j and $\mu^*_{\alpha_j\beta_j}$ its complex conjugate.

From these quantum mechanic operators some observables can be derived [CHO99]. They are linked to the expectation value $\langle . \rangle$ and read:

$$\rho_{e,\alpha_j} := \left\langle a^\dagger_{\alpha_j} a_{\alpha_j} \right\rangle \tag{2.31}$$

$$\rho_{h,\beta_j} := \left\langle b^\dagger_{\beta_j} b_{\beta_j} \right\rangle \tag{2.32}$$

$$\tilde{p}_{\alpha_j,\beta_j} := \left\langle b_{\beta_j} a_{\alpha_j} \right\rangle = \left\langle a^\dagger_{\alpha_j} b^\dagger_{\beta_j} \right\rangle^*, \tag{2.33}$$

where ρ_{e,α_j} (ρ_{h,β_j}) is the average electron (hole) occupation probability in state α_j (β_j) and $\tilde{p}_{\alpha_j,\beta_j}$ is the microscopic dipole polarization amplitude for the optical transition α_j-β_j. The time evolution can now be obtained either in the Heisenberg representation of quantum mechanics or through the Ehrenfest theorem, for details

see Ref. [SCU97]. The expectation value of an operator $\hat{o}$ then changes according to:

$$\frac{\partial}{\partial t}\langle\hat{o}\rangle = \frac{i}{\hbar}\left\langle\left[\hat{H}(t)\hat{o}(t)\right]\right\rangle = \hat{H}(t)\hat{o}(t) - \hat{o}(t)\hat{H}(t). \tag{2.34}$$

With [.] denoting the commutator as shown above. Hence, for the time evolution of the observables in Eq. (2.33) the commutator with the Hamiltonian has to be evaluated. This is a tedious calculation, which will not be shown here, where the anticommutator relation for fermions has to be used several times:

$$\left\{a_m^\dagger, a_n\right\} := a_m^\dagger a_n + a_n a_m^\dagger = \delta_{mn}. \tag{2.35}$$

At the end, the following differential equations are obtained:

$$\frac{\mathrm{d}\tilde{p}_{\alpha_j\beta_j}}{\mathrm{d}t} = -i\omega_{\alpha_j\beta_j}\tilde{p}_{\alpha_j\beta_j} - \frac{i}{\hbar}\mu_{\alpha_j\beta_j}\mathrm{Re}\left(E(t)e^{-i\omega t}\right)\left(\rho_{e,\alpha_j} + \rho_{h,\beta_j} - 1\right) \tag{2.36}$$

$$\frac{\mathrm{d}\rho_{e,\alpha_j}}{\mathrm{d}t} = \frac{\mathrm{d}\rho_{h,\beta_j}}{\mathrm{d}t} = -\frac{i}{\hbar}\left(\mu^*_{\alpha_j\beta_j}\tilde{p}^*_{\alpha_j\beta_j} - \mu_{\alpha_j\beta_j}\tilde{p}_{\alpha_j\beta_j}\right)\mathrm{Re}\left(E(t)e^{-i\omega t}\right), \tag{2.37}$$

where $\omega_{\alpha_j\beta_j}$ is the frequency of the transition α_j-β_j. Then, the microscopic polarization $\tilde{p}_{\alpha_j\beta_j}$ amplitude can be transformed into a new variable $p_{\alpha_j\beta_j}$, describing the slowly varying amplitude in a rotating frame with the same frequency ω as the incoming electric field:

$$\tilde{p}_{\alpha_j\beta_j} =: p_{\alpha_j\beta_j}e^{-i\omega t}. \tag{2.38}$$

And the time evolution of this new variable is given by:

$$\frac{\mathrm{d}\tilde{p}_{\alpha_j\beta_j}}{\mathrm{d}t} = \frac{\mathrm{d}p_{\alpha_j\beta_j}}{\mathrm{d}t}e^{-i\omega t} - i\omega p_{\alpha_j\beta_j}e^{-i\omega t}. \tag{2.39}$$

This can now be used together with the expansion of $\mathrm{Re}\left(E(t)e^{-i\omega t}\right)$:

$$\mathrm{Re}\left(E(t)e^{-i\omega t}\right) = \frac{1}{2}\left(E(t)e^{-i\omega t} + E^*(t)e^{i\omega t}\right), \tag{2.40}$$

and inserting Eq. (2.39) and Eq. (2.40) into Eq. (2.37), while using the definition of $p_{\alpha_j\beta_j}$ yields:

$$\frac{\mathrm{d}p_{\alpha_j\beta_j}}{\mathrm{d}t} = -i\left(\omega_{\alpha_j\beta_j} - \omega\right)p_{\alpha_j\beta_j} - \frac{i}{2\hbar}\mu_{\alpha_j\beta_j}\left(E(t) + E^*(t)e^{i2\omega t}\right)\left(\rho_{e,\alpha_j} + \rho_{h,\beta_j} - 1\right) \tag{2.41}$$

$$\frac{\mathrm{d}\rho_{e,\alpha_j}}{\mathrm{d}t} = \frac{\mathrm{d}\rho_{h,\beta_j}}{\mathrm{d}t} = -\frac{i}{2\hbar}\left(\mu^*_{\alpha_j\beta_j}p^*_{\alpha_j\beta_j}e^{i\omega t} - \mu_{\alpha_j\beta_j}p_{\alpha_j\beta_j}e^{-i\omega t}\right)\left(E(t)e^{-i\omega t} + E^*(t)e^{i\omega t}\right). \tag{2.42}$$

These equations now contain terms oscillating with frequency 2ω. As the intrinsic time scales of the polarization amplitude $p(t)$ and electric field amplitude $E(t)$ are several orders of magnitude larger, these fast oscillating terms can be neglected. On these long time scales, they average out to zero. Additionally, the Rabi-frequency $\Omega_{\alpha_j\beta_j}$ is introduced as:

$$\Omega_{\alpha_j\beta_j}(t) = \frac{\mu_{\alpha_j\beta_j} E(t)}{\hbar}, \tag{2.43}$$

so that the semiconductor-Bloch-equations are finally derived:

$$\frac{\mathrm{d}p_{\alpha_j\beta_j}}{\mathrm{d}t} = -i\left(\omega_{\alpha_j\beta_j} - \omega\right) p_{\alpha_j\beta_j} - \frac{i\Omega_{\alpha_j\beta_j}}{2}\left(\rho_{e,\alpha_j} + \rho_{h,\beta_j} - 1\right) - \frac{1}{T_2} p_{\alpha_j\beta_j} \tag{2.44}$$

$$\frac{\mathrm{d}\rho_{e,\alpha_j}}{\mathrm{d}t} = \frac{\mathrm{d}\rho_{h,\beta_j}}{\mathrm{d}t} = -\operatorname{Im}\left(\Omega_{\alpha_j\beta_j} p^*_{\alpha_j\beta_j}\right) + R^m_{sp} + R^m_{scat} \tag{2.45}$$

Here, some additional phenomenological terms have been added. In addition to the coherent dynamics as derived from the Hamiltonian, the polarization amplitude p decays with the dephasing time T_2, accounting for the decay due to scattering processes such as carrier-carrier scattering [KOC00] and carrier-phonon scattering. Furthermore, the carrier densities ρ_{e,α_j} and ρ_{h,β_j} are subject to losses due to spontaneous emission R_{sp} and input and output R_{scat} by carrier scattering. The final forms for these terms used in this works will be shown later.

But first, the notation will be simplified to more closely match the two-state lasing quantum dots. Therefore, the indeces α_j and β_j will be replaced by $m \in \{GS, ES\}$, sorting everything into QD excited state (ES) and ground state (GS) variables. Furthermore, it will be assumed that only these two transitions are active, so that $\mu_{\alpha_j\beta_j} = 0$ and $p_{\alpha_j\beta_j} = 0$ for all other recombination processes. The notation then reads:

$$\begin{aligned} p^m &:= p_{\alpha_j\beta_j} \\ \rho^m_e &:= \rho_{e,\alpha_j} \\ \rho^m_h &:= \rho_{e,\beta_j} \\ \Omega^m &:= \Omega_{\alpha_j\beta_j} = \frac{\mu^m E^m(t)}{\hbar} \end{aligned} \tag{2.46}$$

Now, the polarization dynamics in QD lasers are very fast [CHO99, BIM08a]. Hence, for the description on time-scales larger than the microscopic dephasing time, they can be adiabatically eliminated. It will therefore be assumed, that the polarization relaxes at all times to a value as given by the other variables. By setting the time evolution of the complex conjugated p^{m*} to zero,

$$0 = \frac{\mathrm{d}p^{m*}}{\mathrm{d}t} = \frac{i\Omega^{m*}}{2}\left(\rho^m_e + \rho^m_h - 1\right) - \frac{1}{T_2} p^{m*}, \tag{2.47}$$

and solving for the value of p^{m*},

$$p^{m*} = iT_2\Omega^{m*}\left(\rho_e^m + \rho_h^m - 1\right), \tag{2.48}$$

the semiconductor Bloch-equations can be reduced to the two differential equations for ρ^m and their final form can be obtained:

$$\begin{aligned}\frac{\mathrm{d}\rho_b^m}{\mathrm{d}t} =& -\operatorname{Im}\left(\Omega^{m*}p^{m*}\right) + R_{sp} + R_{scat} \\ =& T_2\frac{|\mu^m|^2}{\hbar^2}|E^m|^2\left(\rho_e^m + \rho_h^m - 1\right) + R_{sp} + R_{scat}\end{aligned} \tag{2.49}$$

Finally, the result for the steady state of p^{m*} given in Eq. (2.48) can be used to calculate the macroscopic polarization P^m:

$$P^m(t) = \mu^m Z^{QD} p^m(t). \tag{2.50}$$

Here Z^{QD} denotes the number of quantum dots in the active medium, while μ^m is, as before, the microscopic polarization of the transition. The macroscopic polarization P^m is the dynamic variable that was missing in the description of the electric field dynamics given in Eq. (2.29). When inserting, the electric field equation is obtained as:

$$\begin{aligned}\frac{\mathrm{d}E^m}{\mathrm{d}t} =& \frac{i\omega\Gamma}{2\epsilon_0\epsilon_{bg}}P^m \\ =& \frac{\omega\Gamma T_2\nu_m Z^{QD}|\mu^m|^2}{2\epsilon_0\epsilon_{bg}\hbar}E^m\left(\rho_e^m + \rho_h^m - 1\right) \\ =& gE^m\left(\rho_e^m + \rho_h^m - 1\right),\end{aligned} \tag{2.51}$$

where the prefactor g denotes the optical gain. However, this only models the stimulated emission, and followingly the addiion of a spontaneous emission term will be covered in the next section.

2.2.3. Modelling of Spontaneous Emission

For the carrier occupation probabilities ρ_e^m and ρ_h^m, the loss by spontaneous recombination of electron-hole pairs can be modelled deterministically by using the Einstein-coefficients for spontaneous emission W_m:

$$R_{sp}^m = -W_m\rho_e^m\rho_h^m. \tag{2.52}$$

Followingly, photons are emitted at the same rate. But not all photons that are spontaneously emitted, are emitted in the right direction or polarization, so that

many of them do not add to the number of photons N^{ph} in the lasing mode. Only the fraction β [HAK86] is emitted to further the lasing process, therefore Eq. (2.52) has to be modified accordingly for calculating the spontaneous emission contribution $\partial_t N_{sp}^{ph,m}$ to the photon number:

$$\partial_t N_{sp}^{ph,m} = \nu_m \beta Z^{QD} W_m \rho_e^m \rho_h^m. \tag{2.53}$$

Here, Z^{QD} denotes the number of quantum dots that are emitting and ν_m is the degeneracy of the level m. The rate of photon creation in Eq. (2.53) now has to be converted into electric field amplitude change. This is done by assuming energy conservation, for which the conversion between photons N^{ph} and electric field amplitude E is given by:

$$\frac{V_{mode}}{2} \epsilon_0 \epsilon_{bg} \partial_t |E_{sp}|^2 = \hbar\omega \partial_t N_{sp}^{ph}, \tag{2.54}$$

where V_{mode} denotes the spatial extent of the electric field mode:

$$V_{\mathrm{mode}} = \frac{A h a_{\mathrm{l}}}{\Gamma}, \tag{2.55}$$

and A is the in-plane area of the active medium, e.g. the quantum dot layer, h is the height of one active medium layer, a_{l} is the number of layers and Γ is the confinement factor.

Accordingly, the change of energy in the mode has to be the same for both photons and electric field, so that:

$$\partial_t N_{sp}^{ph,m} = \beta \nu_m W_m \rho_e^m \rho_h^m = \frac{V_{mode} \epsilon_0 \epsilon_{bg}}{2\hbar\omega} \partial_t |E_{sp}|^2, \tag{2.56}$$

where Eq. (2.53) was used. This can now be reshuffled to yield an expression for $\partial_t |E_{sp}|^2$:

$$\partial_t |E_{sp}|^2 = \nu_m \beta Z^{QD} W_{GS} \eta_{GS}^2 \rho_e^{GS} \rho_h^{GS}, \tag{2.57}$$

describing the time evolution due to spontaneous emission of the amplitude square $|E_{sp}|^2$, where η_m^2 is the conversion factor between electric field amplitude and photon number N^{ph}, which is given by:

$$\eta_m^2 = \frac{(2\hbar\omega_m)}{(V_{\mathrm{mode}} \epsilon_{bg} \epsilon_0)}. \tag{2.58}$$

In a last step, the derivative for the intensity $\partial_t |E|^2$ has to be converted into electric field amplitude change [FLU07]:

$$\partial_t E = \frac{E}{2|E|^2}\partial_t |E|^2 \tag{2.59}$$

Thus, the resulting spontaneous emission term is:

$$\partial_t E_{sp} = \beta Z^{QD} W_{GS} \eta_{GS}^2 \rho_e^{GS} \rho_h^{GS} \frac{E^{GS}}{|E^{GS}|^2}. \tag{2.60}$$

This can now be added to the field equation of Eq. (2.51). The complete set of rate equations will be presented in the next section.

2.3. Model of a Quantum Dot Laser

2.3.1. Dynamical Equations

After the full matter and electric field equations have been derived in the previous section, their final form shall be presented here. Although there exists a wide variety of more complex modelling approaches [CHO13], e.g. taking the k-distribution of carriers in the QW-reservoir into account [LIN11b], previous studies [LIN10] have shown that a simple rate equation approach is sufficient for the scope of this work. The numerical model used is based on previous works [MAJ11, LIN13, LIN14]. It includes the ground state (GS) and excited state (ES) variables for the electric field E^m, electron ρ_e^m and hole occupation probability ρ_h^m, with $m \in \{GS, ES\}$. The reservoir carrier densities w_e and w_h for holes and electrons are modelled as well.

In addition to the semiclassical laser equations derived from light-matter interaction of the previous section, some phenomenological terms have been added to account for additional processes, e.g. spontaneous emission, which will be explained in the following.

First, another feature of QDs must be taken into account: As of today no set of self-assembled QDs consists of identically shaped and sized QDs. Due to the nature of the growth process they exhibit a stochastic distribution of sizes, which in turn changes their confinements and spectral parameters [BIM08a]. This can be measured as a broadening of the collective spectrum, referred to as 'inhomogeneous broadening' (see Fig. 2.7), as compared to the natural linewidth of a single quantum dot (called 'homogeneous broadening'). Yet, only the spectral fraction of QDs with

Table 1: Dynamical variables of the numerical model

Symbol	Values	Meaning
$E^{[GS,ES]}$	$\in \mathbb{C}$	Slowly varying electric field amplitude for GS/ES
$\rho_{[e,h]}^{[ES,GS]}$	$0.0 - 1.0$	ES/GS electron/hole occupation probability for active QDs
$\rho_{[e,h],inact}^{[ES,GS]}$	$0.0 - 1.0$	ES/GS electron/hole occupation probability for inactive QDs
$w_{[e,h]}$	≥ 0	Electron/hole 2D-density in reservoir

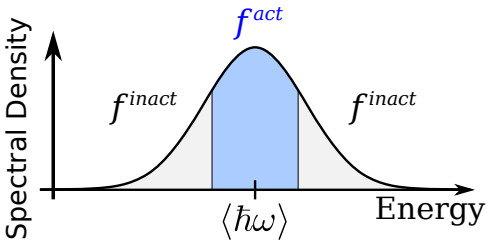

Figure 2.7: Sketch of the emission spectrum of an ensemble of QDs. Due to the self-assembled growth process sizes and therefore transition energies are statistically distributed. To model the effect of this, the ensemble is divided into f^{act} active QDs centered around the main transition energy $\hbar\omega$ and f^{inact} inactive QDs.

the highest density will end up lasing [BIM08a]. As a first and proven valid [LIN14] approximation, the QDs are divided into a fraction of f^{act} optically active and $1 - f^{act} = f_{inact}$ optically inactive QDs (coloured parts in Fig. 2.7). Therefore, a second set of occupations ($\rho^m_{e,inact}$ and $\rho^m_{h,inact}$) is included to account for optically inactive QDs.

The resulting equations for the slowly varying electric field amplitude are:

$$\begin{aligned}\frac{d}{dt}E^{GS} = &\left[g_{GS}\left(\rho_e^{GS}+\rho_h^{GS}-1\right)-\kappa\right]E^{GS}\\ &+\beta Z^{QD} f^{act} W_{GS}\eta_{GS}^2\rho_e^{GS}\rho_h^{GS}\frac{E^{GS}}{|E^{GS}|^2},\end{aligned} \tag{2.61}$$

$$\begin{aligned}\frac{d}{dt}E^{ES} = &\left[g_{ES}\left(\rho_e^{ES}+\rho_h^{ES}-1\right)-\kappa\right]E^{ES}\\ &+\beta Z^{QD} f^{act} W_{ES}\eta_{ES}^2\rho_e^{ES}\rho_h^{ES}\frac{E^{ES}}{|E^{ES}|^2}.\end{aligned} \tag{2.62}$$

The first term accounts for the stimulated emission in accordance with the derivation in Sec. 2.1, where a decay term κE^m was added, accounting for the continuous loss of light intensity at the mirrors and by off-resonant absorption. The linear optical gain $g_{[GS,ES]}$ and decay rate κ are measured in units of $[1/ps]$. The second term deterministically models spontaneous emission. The number of QDs Z^{QD}, the Einstein-coefficient for spontaneous emission $W_{[GS,ES]}$ and the β-factor are without unit. The β-factor is equal to the fraction of spontaneously emitted photons that enter the lasing mode of the resonator, whereas the majority usually is lost.

The final form of the matter equations for the active quantum dots with $b \in \{e, h\}$ are:

$$\begin{aligned}\frac{d}{dt}\rho_b^{GS} = &-\frac{g_{GS}}{\nu_{GS} Z^{QD} f^{act}}\left(\rho_e^{GS}+\rho_h^{GS}-1\right)\frac{|E^{GS}|^2}{\eta_{GS}^2}-W_{GS}\rho_e^{GS}\rho_h^{GS}\\ &+S_{b,in}^{GS,cap}\left(1-\rho_b^{GS}\right)-S_{b,out}^{GS,cap}\left(\rho_b^{GS}\right)\\ &+S_{b,in}^{rel}\left(1-\rho_b^{GS}\right)\rho_b^{ES}-S_{b,out}^{rel}\rho_b^{GS}\left(1-\rho_b^{ES}\right),\end{aligned} \tag{2.63}$$

$$\begin{aligned}\frac{d}{dt}\rho_b^{ES} =& -\frac{g_{ES}}{\nu_{ES} Z^{QD} f^{act}}\left(\rho_e^{ES}+\rho_h^{ES}-1\right)\frac{|E^{ES}|^2}{\eta_{ES}^2} - W_{ES}\rho_e^{ES}\rho_h^{ES} \\ &+ S_{b,in}^{ES,cap}\left(1-\rho_b^{ES}\right) - S_{b,out}^{ES,cap}\left(\rho_b^{ES}\right) \\ &- \frac{1}{2}\left[S_{b,in}^{rel}\left(1-\rho_b^{GS}\right)\rho_b^{ES} - S_{b,out}^{rel}\rho_b^{GS}\left(1-\rho_b^{ES}\right)\right].\end{aligned} \tag{2.64}$$

Inactive QDs experience identical scattering rates, but lack any contribution by stimulated emission. They still emit spontaneously, though most of their emission light leaves the cavity quickly and is then lost:

$$\begin{aligned}\frac{d}{dt}\rho_{b,inact}^{GS} =& - W_{GS}\rho_{e,inact}^{GS}\rho_{h,inact}^{GS} \\ &+ S_{b,in}^{GS,cap}\left(1-\rho_{b,inact}^{GS}\right) - S_{GS,out}^{GS,cap}\left(\rho_{b,inact}^{GS}\right) \\ &+ \left[S_{b,in}^{rel}\left(1-\rho_{b,inact}^{GS}\right)\rho_{b,inact}^{ES} - S_{b,out}^{rel}\rho_{b,inact}^{GS}\left(1-\rho_{b,inact}^{ES}\right)\right],\end{aligned} \tag{2.65}$$

$$\begin{aligned}\frac{d}{dt}\rho_{b,inact}^{ES} =& - W_{ES}\rho_{e,inact}^{ES}\rho_{h,inact}^{ES} \\ &+ S_{b,in}^{ES,cap}\left(1-\rho_{b,inact}^{ES}\right) - S_{b,out}^{ES,cap}\left(\rho_{b,inact}^{ES}\right) \\ &- \frac{1}{2}\left[S_{b,in}^{rel}\left(1-\rho_{b,inact}^{GS}\right)\rho_{b,inact}^{ES} - S_{b,out}^{rel}\rho_{b,inact}^{GS}\left(1-\rho_{b,inact}^{ES}\right)\right].\end{aligned} \tag{2.66}$$

2D-reservoir variables w_e and w_h are measured in units of $[1/nm^2]$ and count charge carriers per area. The reservoir is filled with a constant influx of carriers by the current density J and decays at a rate of R_{loss}^W, which models all radiative and non-radiative loss processes. The scattering processes are weighted according to the area density of QDs N^{QD} given and the degeneracy of the levels (2 for GS, 4 for ES):

$$\frac{d}{dt}w_b = + J - R_{\text{loss}}^W w_e w_h \tag{2.67}$$

$$\begin{aligned}&- 2N^{QD} f^{act}\left[S_{b,in}^{GS,cap}(1-\rho_b^{GS}) - S_{b,out}^{GS,cap}(\rho_b^{GS})\right] \\ &- 4N^{QD} f^{act}\left[S_{b,in}^{ES,cap}(1-\rho_b^{ES}) - S_{b,out}^{ES,cap}(\rho_b^{ES})\right] \\ &- 2N^{QD}(1-f^{act})\left[S_{b,in}^{GS,cap}(1-\rho_{b,ia}^{GS}) - S_{b,out}^{GS,cap}(\rho_{b,ia}^{GS})\right] \\ &- 4N^{QD}(1-f^{act})\left[S_{b,in}^{ES,cap}(1-\rho_{b,ia}^{ES}) - S_{b,out}^{ES,cap}(\rho_{b,ia}^{ES})\right],\end{aligned} \tag{2.68}$$

For visualization, a sketch of the energy band structure and scattering processes of the QD model is shown in Fig. 2.8. The energy spacing for electrons and holes is

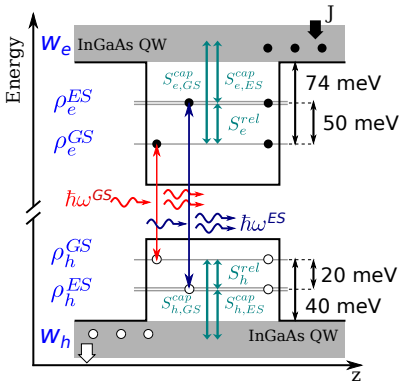

Figure 2.8: Sketch of the energy band structure, scattering processes and optical transition of the QD model. J denotes the pump current, ρ_b^m are occupation probabilities and w_b are the 2D-reservoir densities. There is an asymmetric energy spacing for electrons (e) and holes (h). The excited state (ES) has a degeneracy of two. ©(2015) IEEE. Reprinted, with permission, from [ROE14]

different, enabling asymmetric carrier dynamics. Injection current J only enters the system in the 2D-reservoir densities w_b. Recombination of GS electron-hole pairs and ES electron-hole pairs are the two lasing transitions described by the numerical model with E^{GS} and E^{ES}. Spin degeneracy is generally suppressed, but the ES level is assumed to be twice degenerate in comparison to the GS.

Table 2: Parameters for the QD model.

Symbol	Value	Meaning
$\hbar\omega_{GS}$	0.952eV	GS transition energy
$\hbar\omega_{ES}$	1.022eV	ES transition energy
a_L	15	number of QD layers
l	1mm	device length
d	2.4μm	device width
h	4nm	height of one layer
Γ	0.05	confinement factor
ϵ_{bg}	14.2	background permittivity
η_{GS}	9.157×10^{-7}V/nm	electric field conversion factor (GS)
η_{ES}	9.51×10^{-7}V/nm	electric field conversion factor (ES)

The optical transitions for the GS has an energy of $\hbar\omega_{GS} = 0.952$ eV, while the ES has $\hbar\omega_{ES} = 1.012$ eV. With the device assumed to have length $l = 1$ mm, width $d = 2.4$ μm and 15 active layers of height $h = 4$ nm, the mode volume can be calculated to $V_{\text{mode}} = 2.88 \times 10^{-15}$ m^3 for a confinement factor $\Gamma = 0.05$. The permittivity of GaAs is $\epsilon_{bg} = 14.2$, so that the conversion factors between photon number and electric field amplitude can be calculated. The results are given in Tab. 2, together with the parameters used in the calculation.

Now only the scattering rates need to be described, as is done in the next section.

2.3.2. Scattering Rates

Calculating the scattering rates for a semiconductor is a difficult task, as there are many possible recombination and transition processes in a semiconductor[SCH89]. The scattering rates S used in this work were calculated by a microscopic approach in previous works [MAL07, MAJ11, MAJ12]. The carrier-carrier interactions are modelled by a Born-Markov approximation, while the phonon-scattering is neglected. This leaves room for future improvements, as the phonon-assisted carrier capture might be especially important when an extra ES is included. A typical nonlinear fit of the scattering rates is given by:

$$S_{e,in}^{GS,cap} = \frac{(A_1 w_e^2 + A_2 w_h^2)\exp(C_1 w_e + C_2 w_h)}{1 - B_1 w_h/w_e + B_2 w_e + B_3 w_h - B_4 w_e^2 + B_5 w_h^2 + B_6 w_e w_h}. \tag{2.69}$$

The constants A_i, B_i and C_i are given in App. A.1. The corresponding out-scattering rate is calculated by the *detailed balance condition*: In thermal equilibrium, when in and out-scattering cancel each other, the occupation probabilities of the participating energy levels ρ_1 and ρ_2 are given by the Fermi-distribution:

$$\rho_1 = \frac{1}{\exp(\frac{E_1 - E_F}{k_b T}) + 1}, \tag{2.70}$$

$$\rho_2 = \frac{1}{\exp(\frac{E_2 - E_F}{k_b T}) + 1}, \tag{2.71}$$

where $E_2 > E_1$ are the potential energy of the levels, T is the temperature, k_B is the Boltzmann-constant and E_F is the Fermi-energy. The effective scattering terms in Eq. (2.63) and Eq. (2.64) have to cancel each other:

$$S_{in}(1 - \rho_1)\rho_2 = S_{out}(1 - \rho_2)\rho_1. \tag{2.72}$$

Inserting Eq. (2.71) and reshuffling yields the detailed balance condition in terms of scattering amplitude:

$$\begin{aligned} \frac{S_{out}}{S_{in}} =& \frac{(1 - \rho_1)\rho_2}{(1 - \rho_2)\rho_1} \\ =& \exp(-\frac{E_2 - E_1}{k_b T}), \end{aligned} \tag{2.73}$$

and hence:

$$S_{out} = S_{in}\exp(-\frac{E_2 - E_1}{k_b T}) \tag{2.74}$$

So that only the energy difference $E_2 - E_1$ enters the detailed balance condition, not the absolute energy. Out-scattering is faster for higher temperatures T and smaller energy spacing, i.e. weaker confinement.

Furthermore, QDs of different sizes will later be investigated. To study them a size scaling parameter r will be introduced and scattering rates are calculated for all of the different QD ensembles. Because of computational limitations, only a linearised fit of the microscopically calculated scattering rates is used. This linearised fit is given in App. A.2. Detailed balance, on the other hand, is fully maintained.